In situ X-ray analysis of protein crystals in low-birefringent and X-ray transmissive plastic microchannels

Joseph D. Ng,[a] **Peter J. Clark,**[b] **Raymond C. Stevens**[a] **and Peter Kuhn**[b]*

[a]Department of Molecular Biology, The Scripps Research Institute, 10550 North Torrey Pines Road, La Jolla, CA 92037, USA, and [b]Department of Cell Biology, The Scripps Research Institute, 10550 North Torrey Pines Road, La Jolla, CA 92037, USA

Correspondence e-mail: pkuhn@scripps.edu

Plastic microchannel crystallization template designs made from inexpensive cyclic olefin copolymers have been shown to be low-birefringent, X-ray transmissive and compatible with microfluidic fabrication in restricted geometry. The model proteins thaumatin, lysozyme and bacteriorhodopsin demonstrated the feasibility of conducting counter-diffusion equilibration within the new plastic configuration. Crystals of each of these proteins were directly evaluated *in situ* using synchrotron radiation and their diffraction quality was evaluated without invasive manipulation or cryofreezing. Protein crystals able to produce complete X-ray data sets were used to calculate electron-density maps for structure determination. Fluidic crystallization in the plastic platform was also coupled with a commercialized automated imager and an *in situ* X-ray scanner that allowed optical and X-ray inspection of crystallization hits. The results demonstrate the feasibility of rapid nanovolume counter-diffusion crystallization experiments without the need for additional instrumentation.

1. Introduction

Recent developments of protein crystal growth in small volumes and automation have provided tools to screen protein crystals more efficiently by vapor, liquid–liquid or counter-diffusion equilibration (Santarsiero *et al.*, 2002). Restricted-geometry developments include microfluidic devices (Hansen *et al.*, 2002, 2006; Gerdts *et al.*, 2006; Li *et al.*, 2006), plastic tubings (Kalinin & Thorne, 2005; Yadav *et al.*, 2005) and glass capillaries (García-Ruiz, 2003; Ng *et al.*, 2003, 2008; Gavira *et al.*, 2002; García-Ruiz & Ng, 2007; Yadav *et al.*, 2005). Protein crystals obtained in these systems can be analyzed by X-ray diffraction *in situ* and consequently unit-cell parameters and space groups can be determined. In favorable cases, complete diffraction data sets can be collected, allowing structure determination. All of this is performed without any manual manipulation of the crystal samples.

The goal of this study was to examine plastic template designs prepared from cyclic olefin copolymers (COCs) for counter-diffusion protein crystallization. The plastic construct contained microchannels of different configurations made by micro-injection molding. Microchannels were fabricated for easy counter-diffusion crystallization preparation using between 200 nl and 1.96 μl protein solution for each crystallization experiment. Protein solutions were set up to equilibrate against a precipitating agent by liquid–liquid diffusion in a virtually convection-free environment. A supersaturation gradient was thus formed and a precipitating solution was explored in a broad integrated range of supersaturation for

doi:10.1107/S0907444907060064   **189**

protein crystallization. Crystals obtained along the length of the plastic microchannel chamber were systematically analyzed by *in situ* X-ray analysis.

While the concept and principles of counter-diffusion crystallization are well understood, the material type and format used to restrict geometry for this process have not been comprehensively explored, especially for automated imaging and *in situ* X-ray analysis. A novel plastic format provides an alternative containment for counter-diffusion equilibration with minimal protein consumption, minimal evaporation and excellent visible and X-ray light-transmission properties. Four of the standard microscope-slide format devices can be mounted in an SBS-size frame for automated imaging and storage. The common model proteins thaumatin, lysozyme and bacteriorhodopsin (bR) were used to represent stable soluble and membrane-associated macromolecules for this effort.

2. Materials and methods

2.1. Proteins and chemicals

Chicken egg-white lysozyme (Cat No. L6876, Lot 051K7028) and thaumatin (Cat No. T7638, Lot 108F0299) were purchased from Sigma–Aldrich (St Louis, Missouri, USA) and used throughout the experiments without further purification. Stock solutions at a final concentration of 50 mg ml^{-1} were prepared for both proteins, consistent with previously published protocols.

Bacteriorhodopsin (bR) was purified from transgenic *Halobacterium halobium* (Oesterhelt & Stoeckenius, 1974). The final protein concentration was determined by measuring the absorbance at 568 nm using a molar extinction coefficient
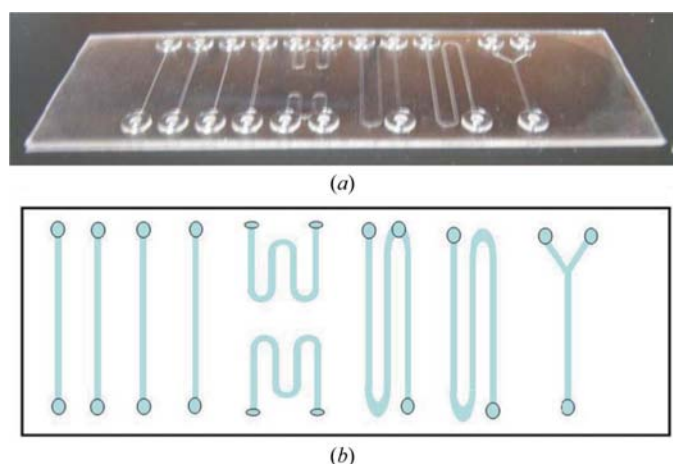

Figure 1
Microchannel plates fabricated by Greiner Bio-One (Frickenhausen, Germany) using micro-injection molding with a cyclic olefin copolymer (COC) plastic. The entire plate is the size of a conventional microscope slide (*a*). Each prototype plate contains nine microchannels with opened filling ports that can hold 0.5 µl in volume. The microchannels are in linear (I), short-turn (M), large-turn (S) and Y configuration as illustrated in (*b*). The channel width ranges from 0.10 to 0.3 mm, with a length of 20–60 mm and a height of 0.1 mm, providing microchannel volumes of 0.2–1.96 µl.

of 63 000 M^{-1} cm^{-1} (Oesterhelt *et al.*, 1973). The final protein solution contained 15 mg ml^{-1} protein, 1.2% *n*-octyl-β-D-glucopyranoside (OG) and 25 mM sodium phosphate buffer pH 5.5.

All reagents used to prepare buffer and precipitating solutions were purchased from Sigma–Aldrich (St Louis, Missouri, USA) or Fluka BioChemika (Buchs, Switzerland). All solutions were made with ultrapure water and the pH was adjusted with 1 M NaOH or 1 M HCl when required and filtered through a 0.22 µm sterile filter (Millipore, Carrigtwohill, Co. Cork, Ireland).

2.2. Plastic constructs

The microchannel plates were fabricated by Greiner Bio-One (Frickenhausen, Germany) using micro-injection molding with a COC-derivatized plastic. The material is low-birefringent, highly transparent and X-ray transmissive and has a sufficient moisture barrier and strength. The COC material has a high chemical resistance to aqueous acids and bases and to most polar solvents. Each prototype device had dimensions of $75 \times 25 \times 1.0$ mm (microscope-slide standard) and the prototypes originally contained nine microchannels of varying configurations as shown in Fig. 1. The width of each microchannel ranged from 0.10 to 0.30 mm, with a length of 20–60 mm. The height was 0.1 mm for each channel. The microchannel volumes were between 200 nl and 1.96 µl protein solution. The ends of the microchannels are opened with a small circular port able to support about 0.5 µl. Consistent with the results of this study, the final plastic construct contains ten straight channels of 2 cm length.

2.3. Crystallization

Counter-diffusion crystallization experiments in microchannel plates were prepared by injecting approximately 0.2–1.96 µl protein solution into the microchannels using a 10 µl Pipetman with a Maxymum Recovery tip that fits tightly into the microchannel ports. The port at the opposite end of the channel was then sealed with Bol-Wax No. 1 (Fluidmaster, San Juan Capistrano, California, USA). The initial entry port was then layered with about 0.5 µl precipitating reagent and sealed with Bol-Wax No. 1. Both ports were permanently sealed with Diamond Shine nail polish (Sally Hansen Del Laboratories Inc., Uniondale, New York, USA).

Lysozyme stock protein solution was prepared at a concentration of 50 mg ml^{-1} in 50 mM sodium acetate pH 4.5 (Lim *et al.*, 1998). The precipitating reagent consisted of the same buffer with 20% sodium chloride. Similarly, thaumatin was prepared at a concentration of 50 mg ml^{-1} in 50 mM sodium phosphate pH 7.0 and its corresponding precipitating solution was 30% sodium tartrate (Ko *et al.*, 1994). In the case of bR, the protein concentration used was 15–20 mg ml^{-1} in the presence of 1.2% OG buffered with sodium phosphate buffer pH 5.5. The membrane protein was set to crystallize against a solution containing 50 mM HEPES pH 7.5 with 30% PEG 2000, 0.1% DDM (*n*-dodecyl β-D-maltoside), 0.02% cholesteryl hemisuccinate and 100 mM NaCl. The crystal-

lization trials of bR were maintained in a dark environment (covered with aluminium at all times) with the exception of imaging and data collection. All crystallization procedures and incubations were performed at room temperature (295 K).

2.4. *In situ* crystal screening and X-ray data analysis

The quality of crystals grown in the microchannel plates was evaluated directly by visual inspection and X-ray diffraction analysis within 5 d. The crystals were observed through a polarized filter under a visible-light microscope. Automated imaging was performed using a digital camera, stitching subsequent images together with *Image-Pro MC* 6.0 software. Crystals grown in microchannel plates were prepared for X-ray analysis by excising one microchannel with a MaxWax Pen plastic heat pen (Kingsley North Inc., Norway, Michigan, USA). The entire length of the plastic channel was then mounted with clay vertically on a standard goniometer head.

Diffraction data were collected using synchrotron radiation tuned to a wavelength of 0.987 Å at Stanford Synchrotron Radiation Laboratory (SSRL) beamline 1-5. Rotation images (1.0°) were collected at a temperature of 283 K. Diffraction data wedges of 25° were collected to identify the best diffracting crystal as judged by the diffraction limit and the mosaicity of the reflection spots. The geometry of the microchannel slides allowed easy positioning and angular accessibility for optimizing data collection. In each case, a single crystal was targeted for complete data collection using a 1.0° rotation angle with an exposure time of 1 s per image. All X-ray data were integrated, scaled and merged using the *HKL*-2000 program package (Otwinowski & Minor, 1997). Data statistics were also obtained using the *CCP*4 program suite (Collaborative Computational Project, Number 4, 1994).

Confined geometries have the additional advantage that optical and X-ray analysis is simplified owing to the well defined location of the crystallization experiment. In addition, using a microscope with an automated stage, the microchannel devices were imaged in both the automated Formulatrix Imager and an Oxford Diffraction Imaging system (Oxford Diffraction, Oxfordshire, England). The microchannel slides were placed in an SBS-format frame for optical imaging and to analyze crystal hits with the integrated PX Scanner device and subsequently with the synchrotron X-ray beam. *In situ* X-ray analysis coupled with visual inspection identifies salt crystals, characterizes diffraction quality and coupled with counter-diffusion experiments provides a new dimension of analysis by evaluating diffraction quality along the counter-diffusion gradient.
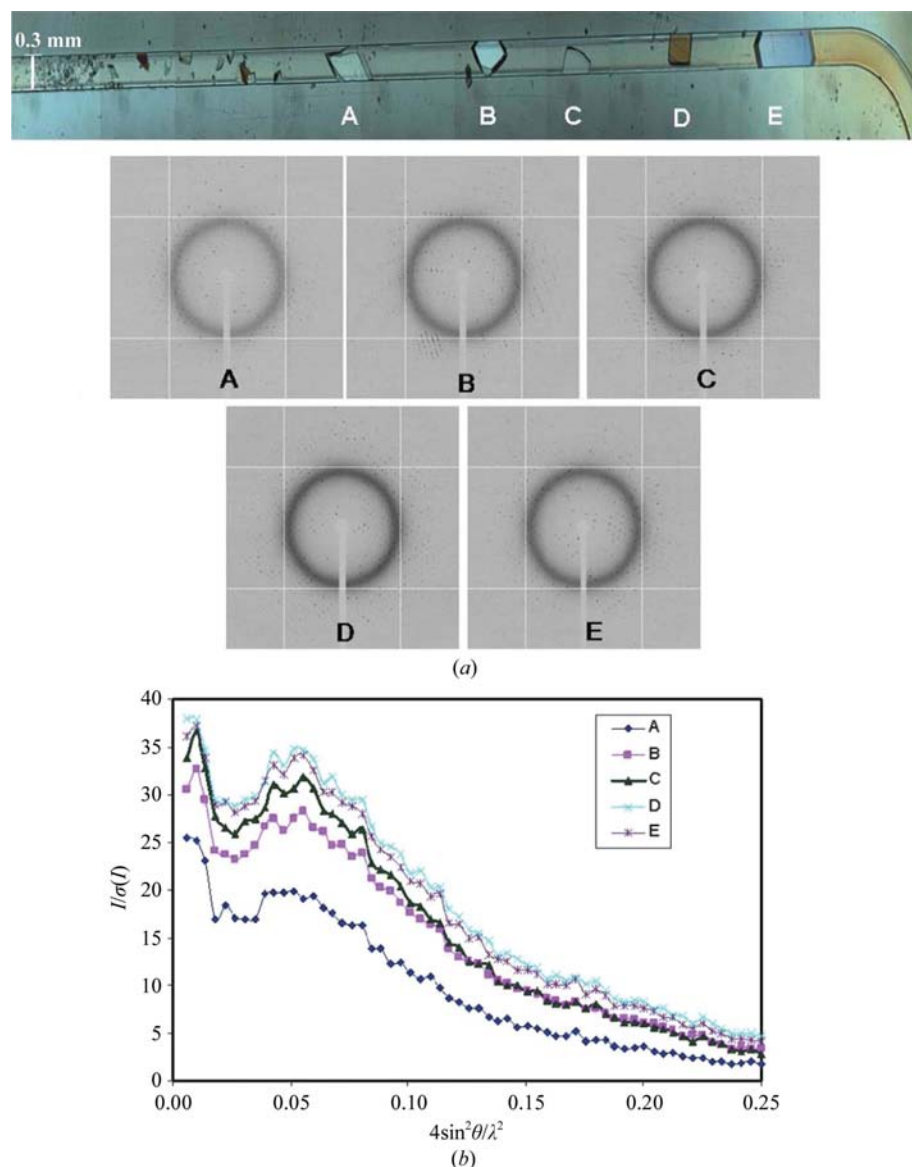

Figure 2
Thaumatin crystals grown along the length of a COC microchannel during the counter-diffusion equilibration process. (*a*) The precipitating solution is diffusing from left to right, creating a supersaturation gradient such that precipitation and high nucleation occurs near the liquid–liquid interface (top left). The number of crystals decreases and the size of each crystal increases along the length of the channel. Crystals can grow and fill up the diameter of the capillary. Crystals A, B, C, D and E were irradiated with synchrotron radiation and the resulting diffraction images are shown in the lower panels. (*b*) X-ray data collection took place for each crystal with 25% completeness of the total number of possible reflections. The quality of each crystal was evaluated by measuring the intensity over noise [$I/\sigma(I)$] as a function of resolution. All the crystals had similar resolution limits, but crystal D had the best intensity over background within the range of resolution examined. Crystal A comparatively had the poorest crystal quality of the five crystals examined and is also the closest single crystal to the precipitant interface.

research papers

2.5. Phasing and initial electron-density map calculations

Complete data sets were only obtained for thaumatin and lysozyme, with fourfold to sevenfold redundancy within each resolution shell. The targeted microchannels could easily be oriented to different χ angles for blind-spot coverage. Initial phasing and electron-density map calculations were performed with complete data sets by molecular-replacement procedures using the program *Phaser* (Read, 2001; Storoni *et al.*, 2004) within the *CCP*4 suite (Collaborative Computational Project, Number 4, 1994). Molecular replacement (MR) was performed *via* a Patterson search method using models of the known targeted protein structures of thaumatin and lysozyme (PDB codes 1thu and 1azf, respectively). Complete data sets were processed and scaled for all $F_o \geq 2\sigma$ between 25 and 2 Å for thaumatin and 50 and 1.76 Å for lysozyme. The orientation of the top solution was refined using the Patterson correlation coefficient of the squared normalized structure factors as the target followed by translation searches.

Initial refinement and electron-density map calculations of the resulting protein models were performed with programs from the *CCP*4 suite. The models and maps were visualized using *Coot* from the same software suite and were illustrated with *PyMOL* (DeLano, 2002).

3. Results and discussion

3.1. Protein crystals

The microchannel plates have the exact dimensions of a standard microscope slide and thus can be immobilized on standard microscope platforms for stability and handling. The prototype microchannels were designed in four types of geometry: linear, M, S and Y configurations (Fig. 1). Protein crystals of thaumatin and lysozyme were observed to appear in all configurations within 3–4 d. Curved channels provided a means of getting a longer capillary onto the slide and showed no difference in counter-diffusion behavior compared with linear channels. The channel with the Y shape was very sensitive to bubble or air-pocket formation, particularly when different precipitating solutions were put in the two arms to diffuse against the protein simultaneously. The supersaturation gradient typically created by counter-diffusion appeared in all the chamber types, indicative of a high number of nucleations near the precipitant–protein interface and fewer and larger crystals appearing along the length of the channel during the equilibration process. The analysis showed that a length of 2 cm is usually sufficient to create a supersaturation range for crystallization screening.

The low and uniform birefringent nature of the microchannel array does not interfere with the identification of crystals grown in the channels under a microscope using a polarizing light filter. Fig. 2(*a*) shows an example of thaumatin crystals grown along the length of the S-shaped channel under polarized light. Usually, distinct prismatic crystals were observed in the linear region, with the largest crystals often filling the entire diameter of the channel. In the case of both thaumatin (Fig. 2) and lysozyme (Fig. 3), single crystals along the length of the microchannel were easily targeted and analyzed by synchrotron radiation to evaluate the quality of the crystals. The excision of the microchannel for X-ray
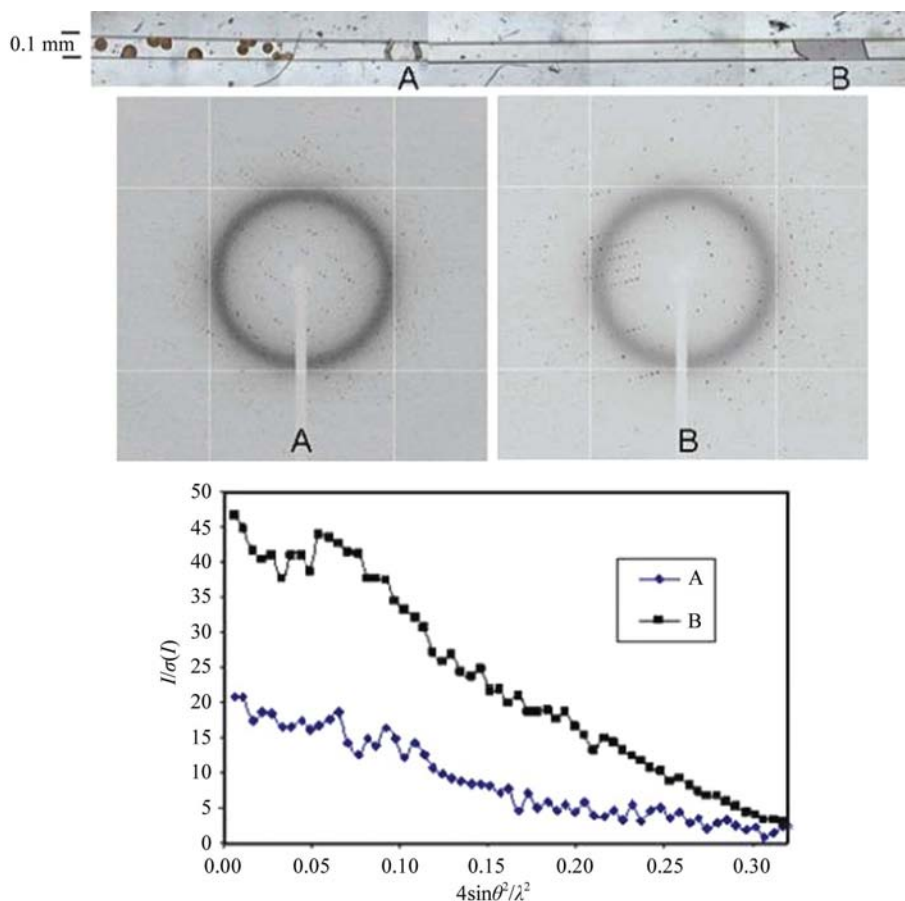

Figure 3
Lysozyme crystals grown along the length of a microchannel in counter-diffusion crystallization. Highly distinguishable crystals were observed along the length of the channel and thus crystals were grown under different supersaturation regimes. The most striking observation was the crystalline balls near the precipitant–protein interface (upper left) and the single crystals then appeared in the middle (A) and at the far right (B). In this case, two crystals grew and filled the volume of the channel. The quality of the crystals differed drastically. Within the resolution examined, the $I/\sigma(I)$ of crystal A was superior to that of crystal B. Relative to the other crystalline features in the channel, crystal B grew most slowly and in the lowest supersaturated area at that particular time. Both crystals A and B were analyzed using synchrotron radiation and the images were collected. The diffraction spots were shown to be less mosaic and extended out further in terms of resolution limit. Subsequently, the structure of lysozyme was determined with the calculation of an initial electron-density map.

analysis did not disturb the experiment; the supersaturation gradient was retained as shown by the precipitation front closest to the precipitant interface and the progression of high to low nucleation of crystal growth along the length of the capillary channel. Any disturbances would have imposed convection and disrupted the supersaturation gradient formation derived from the counter-diffusion process.

Membrane proteins are generally very difficult to crystallize and consequently there are only a handful of structures known compared with soluble proteins. Most membrane-protein crystals have been obtained using conventional methods such as vapor-diffusion, batch or lipid cubic phase methods (Raman *et al.*, 2006). Very few membrane proteins have been used in counter-diffusion experiments, mainly owing to the required presence of lipids and detergents. Moreover, in conventional counter-diffusion experiments in which quartz or X-ray capillaries with a diameter of 0.3 mm are commonly used, a volume of 3–8 μl protein solution at high concentration would be required for each experiment. This is prohibitive for many membrane proteins, which are often only available in limited quantities. In fact, only one prior membrane protein (photosystem II complex) has been crystallized (Kutá Smatanová *et al.*, 2007) by counter-diffusion to date and none has ever been analyzed *in situ*. We have investigated the crystallization behavior of bR by counter-diffusion in microchannels in the presence of detergents and lipids. The same precipitant mixture that gave rise to bR crystals within 2 d by vapor diffusion was used for the counter-diffusion experiment. Similar to thaumatin and lysozyme, bR crystals were observed to be present in all microchannel geometries within 3 d. A precipitation front followed by high crystal nucleation to crystal clusters was observed for bR in the microchannels when the starting protein concentration exceeded 15 mg ml^{-1} (Fig. 4a). The supersaturation gradient formed was very narrow and no single crystals were obtained. However, when the starting concentration of bR was 15 mg ml^{-1} or less, small single crystals could be produced along the supersaturation gradient resulting from the counter-diffusion process along the length of the microchannels (Fig. 4b). The largest bR crystals had an extended needle-like shape and measured about 50 μm in the longest dimension.

Crystals of bR grew to approximately the same size as those grown using a vapor-diffusion setup with the same protein material. The inability to grow large single crystals may be a consequence of the heterogeneous nonuniform detergent–lipid interactions of bR with the protein. Consequently, the crystal morphology, defect densities, crystal size and more importantly diffraction resolution and mosaicity were affected. This phenomenon is of course not unique to bR, but occurs with different degrees of severity for all macromolecules (McPherson, 1999; McPherson *et al.*, 1996; Plomp *et al.*, 2003). Membrane proteins are likely to be more sensitive to chronic heterogeneity caused by instability and irregular detergent or lipid binding. Also, the protein concentration was very limiting during the counter-diffusion process owing to the inability to prepare bR at high concentrations. The protein aggregated when its concentration was greater than 15 mg ml^{-1}.

3.2. X-ray diffraction

The COC material was experimentally found to cause only a light diffusive X-ray scatter ring between 4.5 and 5.5 Å, which compares favorably with typical glass capillaries used in counter-diffusion experiments and substantially outperforms other plastics tested. This low-level background diffraction does not interfere with the subsequent X-ray analysis. The diffraction images of five different thaumatin crystals grown along the channel are shown in Fig. 2(a). The quality of each crystal was determined by evaluating the intensity over background as a function of resolution (Fig. 2b). The quality differences were most notable near the low-resolution range, implying that long-distance lattice packing is mostly affected by the degree of supersaturation.
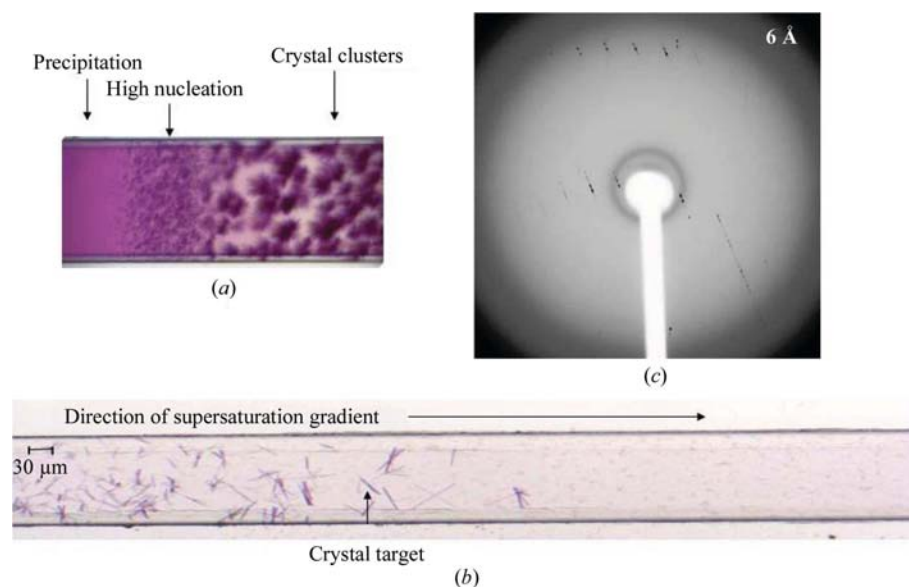

Figure 4
Bacteriorhodopsin crystallization by counter-diffusion observed through plastic microchannels. A very distinct supersaturation gradient is observed indicative of precipitation, high nucleation and crystal-growth regions (a). The established supersaturation gradient is in the direction from left to right. Clusters of crystals were produced when the starting protein concentration was greater than 15 mg ml^{-1}. At protein concentrations of 15 mg ml^{-1} or less, the length of the capillary revealed more distinguishable crystals and a larger number of crystals were observed at the location closest to the precipitant interface (left side). Single crystals ranging from 10 to 50 μm in the longest dimension can be seen and the best crystal target was subjected to X-ray analysis (b). A diffraction photograph of the targeted crystal is shown with reflection spots visible to 6 Å resolution. Distinct lattice reflections are clearly visible(c).

Table 1
Data-processing statistics for thaumatin and lysozyme crystals grown in plastic microchannels.

	Thaumatin	Lysozyme
Space group	$P4_12_12$	$P4_32_12$
Unit-cell parameters (Å)	$a = b = 58.51$,	$a = b = 79.06$,
	$c = 151.24$	$c = 37.93$
Resolution range (Å)	25.0–2.0	50.0–1.7
Lowest shell	25.00–4.30	50.00–3.79
Highest shell	2.07–2.00	1.82–1.76
No. of observations	144768	90830
No. of unique reflections	18409	12424
Completeness (%)		
Overall	98.8	99.7
Lowest shell	96.7	99.9
Highest shell	98.5	99.7
R_{merge} (%)		
Overall	9.5	7.3
Lowest shell	3.9	7.7
Highest shell	34.1	38.1
$\langle I/\sigma(I) \rangle$		
Overall	18.42	27.3
Lowest shell	37.9	49.7
Highest shell	5.0	2.7

In the case of lysozyme, the supersaturation gradient was much more dramatic in that morphological differences were observed in crystals along the length of the crystallization chamber (Fig. 3). Crystalline spheres were grown near the precipitant interface, while crystals with defined shapes developed further away. The best crystal in this case was that with the largest volume and furthest away from the precipitation front. Two large crystals were obtained that grew at a significant distance from each other. The crystals diffracted with a substantial difference in diffraction quality (Fig. 3). However, both crystals have the same diffraction limit, even though the $I/\sigma(I)$ for most of the resolution range measured
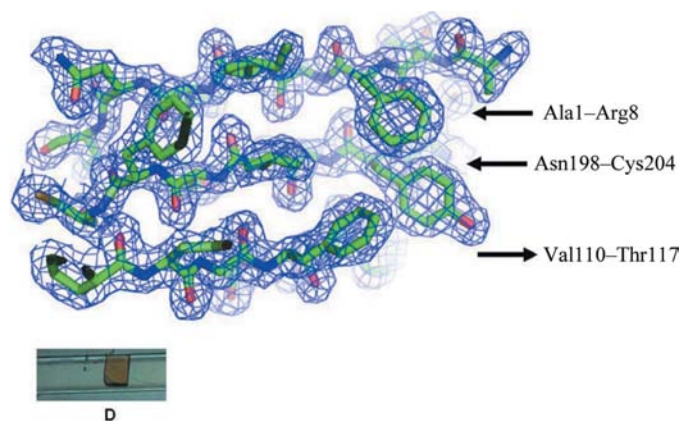
was superior for the more remote crystal. The largest crystal was not necessarily always the best quality in terms of diffraction limit and mosaicity. In almost every instance, relatively poor-quality crystals were situated closest to the precipitant interface and the best were most often observed about three-quarters along the length across the gradient. A key advantage of the counter-diffusion approach as demonstrated here is the ability to systematically investigate the diffraction performance of crystals along the gradient as a reproducible guide to optimizing crystallization conditions.

Crystals of bR were observed to grow along the supersaturation gradient established by counter-diffusion in the plastic microchannel tubes. Even though the bR crystals were very small, the narrow synchrotron X-ray beam was able to target individual crystals obtained along the linear channel. Over 50 crystals were analyzed and none showed any diffraction beyond 20 Å until the crystal targets were situated near the supersaturation front (Fig. 4b). Those that diffracted showed great anisotropy and only revealed partially ordered reflections extending out to 6 Å (Fig. 4c). Since a complete data set could not be collected, it was not possible to quantitatively evaluate the quality of each crystal. Interestingly, when bR was equilibrated against the same precipitant by vapor diffusion, two-dimensional needle-like crystals were obtained within 2 d, none of which diffracted X-rays. While extended studies of bR crystallization with different additives, precipitants, detergents and lipids are in progress, this study demonstrates the feasibility of growing membrane proteins by counter-diffusion in plastic microchannels and its suitability for *in situ* X-ray analysis for crystal evaluation.
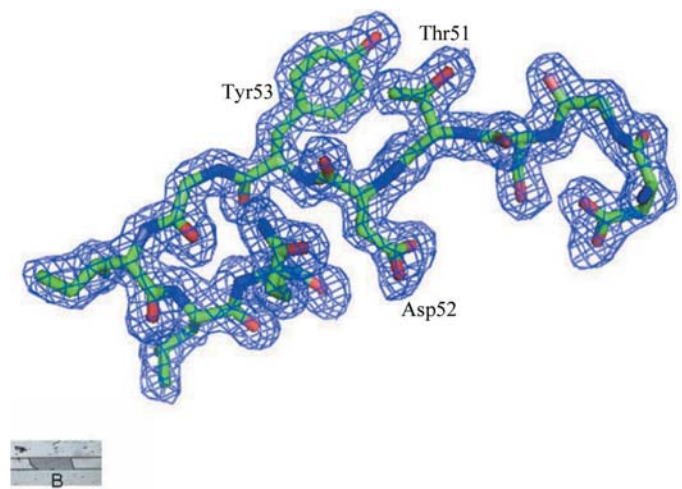

Figure 5
Electron-density map calculated from a complete data set collected *in situ* from a thaumatin crystal grown in plastic microchannels. Crystal D shown in Fig. 2(a) was analyzed using synchrotron radiation. The initial model of thaumatin was determined by molecular replacement and is shown against a calculated $2F_o - F_c$ electron-density map at 2.0 Å. The structure was refined by rigid-body refinement and traced against the experimental density contoured at 1.0σ. The parallel and antiparallel β-sheets containing Ala1–Arg8, Asn198–Cys204 and Val110–Thr117 are shown with arrows indicating the N- to C-terminal directions. The backbone connectivity and side chains are clearly deciphered.

Figure 6
A view of an initial model of lysozyme shown against a $2F_o - F_c$ electron-density map. A complete data set was obtained using synchrotron radiation and the structure of lysozyme was determined by molecular replacement. The map was calculated from a complete data set collected from lysozyme crystal B (shown in Fig. 4) at 1.7 Å resolution. The structure was rigid-body refined and traced against the experimental density contoured at 1.0σ. Only residues 48–57 are shown, including one of the enzyme's active-site residues, Asp52, which is clearly observed between the Try53 and Thr51 residues.

3.3. Crystal to electron density

Complete data sets of the best crystals selected for both thaumatin (Fig. 2a, crystal D) and lysozyme (Fig. 3, crystal B) were collected *in situ* using synchrotron radiation. While the entire microchannel plate could be mounted for X-ray data collection, it proved advantageous for crystal centering and obtaining maximum data completeness to excise each channel and place it on the goniometer. In this manner, nearly 180° of data were collected and used for structure determination. A cold stream under nonfreezing conditions was used to keep the sample environment at constant temperature during data collection. Radiation damage was monitored and data collection was eventually terminated owing to radiation damage. However, it was possible to obtain a high-quality and complete diffraction data set from a single crystal. The reflection spots in the resolution range analyzed were compact, had low mosaic spread and were easily indexed and scaled. Typical data-processing statistics are shown in Table 1. On comparing the X-ray data collected with data collected from crystals in glass capillaries, the data quality was very similar.

Molecular-replacement solutions for thaumatin and lysozyme were easily obtained using the processed *in situ* data against their respective search models. The overall R factors after a single round of rigid-body refinement against the complete protein molecules were 24.2% (R_{free} = 24.0%) and

23.2% (R_{free} = 24.6%) for thaumatin and lysozyme, respectively. The overall figures of merit were above 0.85 for thaumatin and 0.84 for lysozyme. Initial $2F_o - F_c$ maps were calculated without further refinement to demonstrate the feasibility of calculating an initial model using data obtained from X-ray diffraction directly in the microchannel chambers (Figs. 5 and 6). The electron-density maps showed a high degree of connectivity and definition of the solvent region for both protein molecules. Diffraction data were obtained for both protein molecules using synchrotron radiation without the use of cryogenic treatment and their structures were solved easily to resolutions beyond 2 Å.

3.4. Rapid *in situ* X-ray inspection of counter-diffusion crystallization

The counter-diffusion crystallization technique offers the unique advantage of growing protein crystals in a super-saturation gradient such that a single crystallization setup explores a broad range of solubility. As a result, finding conditions for an optimized protein crystal is more probable and the crystal obtained can be prepared for X-ray analysis without additional scale-up or screening. However, in high-throughput applications it is challenging to efficiently visualize and evaluate a large number of experiments by X-ray diffraction. We have explored the possibility of coupling the plastic microchannel crystallization slide to an automated
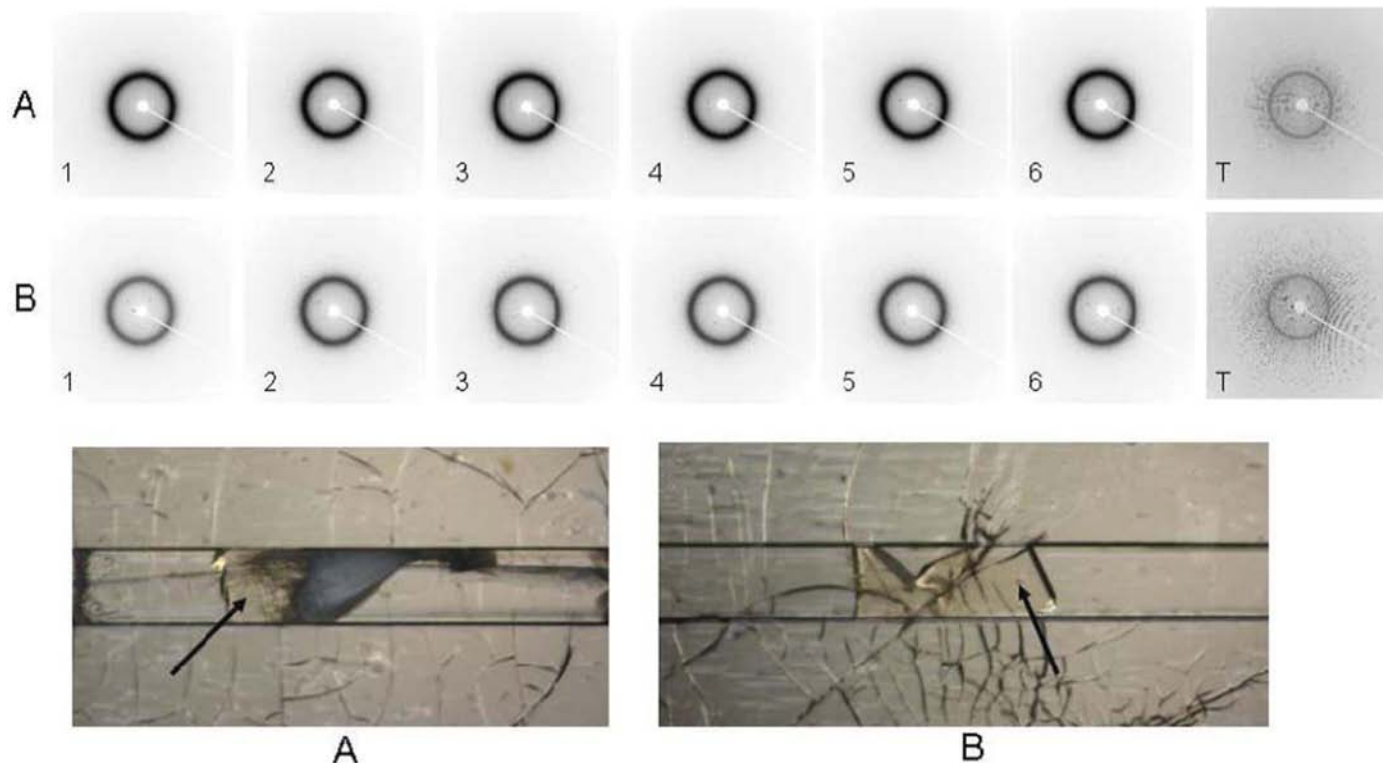

Figure 7
A microchannel crystallization plate was scanned with an automated X-ray scanner. Two thaumatin crystals grown in a microchannel by counter-diffusion equilibration are targeted for optical inspection and *in situ* diffraction. Panels A1–6 are diffraction images of crystal A (bottom left panel), focusing on the crystal area indicated by the arrow. Each frame is a 1 min exposure with an oscillation of 0.25°. Panel AT shows the total images superimposed. Crystal B is analyzed in the same way. The diffraction images show a better quality crystal with higher resolution and finer mosaicity. Crystal B was grown along the microchannel at about three-quarters of the length of the expected supersaturation gradient.

X-ray scanner (PX Scanner, Oxford Diffraction), thus combining optical inspection and *in situ* diffraction. Thaumatin crystals grown in the multi-channel plates described in this paper were stabilized on an *xy* stage to translate the configuration for easy visualization in the PX Scanner. We showed for the first time that protein crystals grown by counter-diffusion in a microvolume plastic array can be inspected with an optical microscope, scanned using X-rays produced by a microfocus X-ray source and their diffraction recorded on a CCD detector. In this proof of concept, we chose to examine thaumatin crystals grown in one of the linear microchannels with 0.3 mm width. Diffraction images were collected at increments of 0.25° (Fig. 7). Two crystals grown at different distances along the length of the channel were analyzed. A total of six images were collected for each crystal, representing a scan of 1.5°. The quality of the crystal can clearly be distinguished in terms of the diffraction quality and resolution limit as seen from the superimposed images. Similarly, crystals of lysozyme were imaged in this format, providing rapid preliminary diffraction images. Thus, it is feasible to examine a multitude of microchannel volumes containing protein crystals in minutes where it would have otherwise taken hours by conventional methods. The primary use of this approach is in the support of optimizing crystallization conditions. Plastic microchannels containing bR were more challenging to image with the PX scanner as crystals were small and inherently did not diffract well, which was consistent with the results obtained by synchrotron-radiation analyses.

4. Conclusion

Previously, a variety of materials were evaluated for *in situ* X-ray diffraction analysis of protein crystals and the use of COC was the most ideal given the minimal vapor permeability and maximal X-ray transmission and light-transparency requirements. Microchannels fabricated with this material can replace glass capillaries, minimizing concerns of fragility and

Figure 8
Microchannel crystallization plates placed in SBS-format frames. The final production microchannel slides contain only 2 cm long linear channels with improved loading ports. The format allows easy viewing, transport and storage. The length of the channel also enables mounting on most current automated goniometer heads at synchrotron beamlines with sufficient travel to scan along the channel.

leading to easy storage of experiments. In the plastic microchannels, counter-diffusion crystallization experiments can be performed with minimal amounts of protein for *in situ* X-ray analysis. Proteins can be screened or optimized in a counter-diffusion regime and directly used for X-ray diffraction without the need for scale-up procedures.

Previous demonstrations of the use of counter-diffusion processes to perform *de novo* crystallization screening involved the utilization of 48–96 precipitating solutions in glass capillaries (Ng *et al.*, 2003). Each capillary screen required at least 3–4 µl if a 0.1 mm diameter capillary tube was used. Therefore, to complete a preliminary crystallization screen would require at least 300 µl (accounting for residual waste) of concentrated purified protein. In the device reported here, we estimated that the amount of protein required for a *de novo* crystallization screen would be 30 µl.

Coupling advanced technology in visualization and automated *in situ* X-ray scanning procedures with microchannel crystallization is ideal for growing and evaluating crystals rapidly with a high amount of correlated information about the experiment. The non-invasive nature of visualizing and using protein crystals for data collection without any physical handling will be particularly important as protein targets become more sensitive and have low tolerance to physical manipulation.

It is worth mentioning that a significant amount of protein crystal damage is often attributed to manual handling and cryofreezing. Consequently, many crystals are discarded during preliminary X-ray screening processes because they show high mosaicity or other types of inferior crystalline characteristics where the protein would have diffracted well otherwise. One of the important points of this study was to show that the crystal quality can be easily evaluated without considering the negative effects of invasive treatment such as those caused by cryogenic treatment. The screening process described here reveals a true evaluation of the crystal quality.

In recent years, a number of devices have become available that allow proteins to grow from free-interface diffusion in nanolitre amounts inside microfluidic chips (*e.g.* Hansen *et al.*, 2002, 2006). While many parallel reactions can be prepared and executed simultaneously in microfluidic chips, there are significant differences in using the new device reported here. Firstly, no pressurization is required for sample loading. Protein and precipitating solutions can be easily loaded with a common manual single-channel or multi-channel micropipette dispenser, requiring no additional dispensing device. Secondly, crystallization conditions found in microchips require further optimization on a larger scale before crystals suitable for complete X-ray data set collection and structure determination can be obtained. Thirdly, the material for the device has a substantially lower evaporation profile. Lastly, *in situ* X-ray analysis for structure determination can be performed directly with the new device. Other microfluidic devices have demonstrated the possibility of *in situ* X-ray data analysis of protein crystals (Li *et al.*, 2006; Gerdts *et al.*, 2006; Yadav *et al.*, 2005). However, these techniques were limited to plug-based designs or batch droplets in which a single supersaturation

point can be screened at a time. In the counter-diffusion configuration, the precipitant and protein solutions are allowed to diffuse against each other such that a spatial–temporal gradient of supersaturation is created. Consequently, during the equilibration process a supersaturation state with respect to the protein can be attained in an integrated labile region of the solubility profile while crystal growth can occur in a continuous range within the metastable conditions. Supersaturation conditions in most plug-based and micro-batch preparations can only target a single labile region for spontaneous nuclei and metastable region for optimal crystal growth (García-Ruiz, 2003; Ng *et al.*, 2003; García-Ruiz & Ng, 2007).

The ability to lay out microchannels in a platform array allows convenient visualization and X-ray screening. The microchannel arrays were designed within the area of a microscope slide such that multiple configurations can be conveniently placed in SBS-format frames as shown in the final microchannel plastic slides (Fig. 8). Since this study demonstrated that the type of channel configuration does not affect the counter-diffusion crystallization results, only linear channels were selected for convenience of fabrication and imaging. Plastic slides in this configuration can easily be transported and stored.

References

Collaborative Computational Project, Number 4 (1994). *Acta Cryst.* D**50**, 760–763.
DeLano, W. L. (2002). *The PyMOL Molecular Graphics System.* DeLano Scientific, San Carlos, CA, USA.
García-Ruiz, J. M. (2003). *Methods Enzymol.* **368**, 130–154.
García-Ruiz, J. M. & Ng, J. D. (2007). *Protein Crystallization Strategies For Structural Genomics*, edited by N. E. Chayen, pp. 111–124. La Jolla, USA: International University Line.
Gavira, J. A., Toh, D., Lopéz-Jaramillo, J., García-Ruíz, J. M. & Ng, J. D. (2002). *Acta Cryst.* D**58**, 1147–1154.
Gerdts, C., Tereshko, V., Yadav, M., Dementieva, I., Collart, F., Joachimiak, A., Stevens, R., Kuhn, P., Kossiakoff, A. & Ismagilov, R. (2006). *Angew. Chem. Int. Ed.* **45**, 8156–8160.
Hansen, C. L., Classen, S., Berger, J. M. & Quake, S. R. (2006). *J. Am. Chem. Soc.* **128**, 3142–3143.
Hansen, C. L., Skordalakes, E., Berger, J. M. & Quake, S. R. (2002). *Proc. Natl Acad. Sci. USA*, **99**, 16531–16536.
Kalinin, Y. & Thorne, R. (2005). *Acta Cryst.* D**61**, 1528–1532.
Ko, T.-P., Day, J., Greenwood, A. & McPherson, A. (1994). *Acta Cryst.* D**50**, 813–825.
Kutá Smatanová, I., Gavira, J. A., Rezácová, P., Vácha, F. & García-Ruiz, J. M. (2007). *Photosynth. Res.* **90**, 255–259.
Li, L., Mustafi, D., Fu, Q., Tereshko, V., Chen, D. L., Tice, J. D. & Ismagilov, R. F. (2006). *Proc. Natl Acad. Sci. USA*, **103**, 19243–19248.
Lim, K., Nadarajah, A., Forsythe, E. L. & Pusey, M. L. (1998). *Acta Cryst.* D**54**, 899–904.
McPherson, A. (1999). *Crystallization of Biological Macromolecules.* New York: Cold Spring Harbor Laboratory Press.
McPherson, A., Malkin, A. J., Kuznetsov, Y. G. & Koszelak, S. (1996). *J. Cryst. Growth*, **168**, 74–92.
Ng, J. D., Gavira, J. A. & García-Ruiz, J. M. (2003). *J. Struct. Biol.* **142**, 218–231.
Ng, J. D., Stevens, R. C. & Kuhn, P. (2008). *Methods in Molecular Biology*, Vol. 426, *Structural Proteomics: High-throughput Methods*, edited by B. Kobe, M. Guss & T. Huber. Totowa: Humana Press Inc. In the press.
Oesterhelt, D., Meentzen, M. & Schuhmann, L. (1973). *Eur. J. Biochem.* **40**, 453–463.
Oesterhelt, D. & Stoeckenius, W. (1974). *Methods Enzymol.* **31**, 667–678.
Otwinowski, Z. & Minor, W. (1997). *Methods Enzymol.* **276**, 307–326.
Plomp, M., McPherson, A. & Malkin, A. J. (2003). *Proteins*, **50**, 486–495.
Raman, P., Cherezov, V. & Caffrey, M. (2006). *Cell. Mol. Life Sci.* **63**, 36–51.
Read, R. J. (2001). *Acta Cryst.* D**57**, 1373–1382.
Santarsiero, B. D., Yegian, D. T., Lee, C. C., Spraggon, G., Gu, J., Scheibe, D., Uber, D. C., Cornell, E. W., Nordmeyer, R. A., Kolbe, W. F., Jin, J., Jones, A. L., Jaklevic, J. M., Schultz, P. G. & Stevens, R. C. (2002). *J. Appl. Cryst.* **35**, 278–281.
Storoni, L. C., McCoy, A. J. & Read, R. J. (2004). *Acta Cryst.* D**60**, 432–438.
Yadav, M. K., Gerdts, C. J., Sanishvili, R., Smith, W. W., Roach, L. S., Ismagilov, R. F., Kuhn, P. & Stevens, R. C. (2005). *J. Appl. Cryst.* **38**, 900–905.